

## Anonymous Referee #1

In this paper, volume emission rate of the 630-nm airglow is calculated using the SAMI2 model, which is a numerical model of the ionosphere. The authors investigate effects of the neutral winds and temperatures on the volume emission rate, but their argument is still only qualitative. This reviewer considers that quantitative investigation is needed. Therefore, major revision is needed before its publication.

We would like to thank Referee #1 for reading our article carefully and providing us helpful and valuable suggestions for improving our manuscript. About quantitative investigation, we have added new figures (Fig. 4) and addressed it in detail in our manuscript. We have also revised the manuscript accordingly by taking into account the Referee's comments. We hope that Referee #1 now finds the manuscript acceptable for publication.

Although the authors describe that effect of the meridional neutral wind is dominant, it is obvious from the equation of the volume emission rate because the volume emission rate is proportional to a product of the plasma and atomic oxygen densities. Meridional neutral winds move the plasma along the magnetic field line and modify plasma density distribution. Consequently, effects of the neutral winds is dominant. This reviewer recommends the author to calculate the 630-nm airglow intensity by integrating the volume emission rate along the altitude, and show it as a function of the neutral temperature and meridional neutral winds. The, the authors should argue quantitatively how much the neutral temperature affect the 630-nm airglow intensity compared to the effects of the neutral winds.

Thanks for Referee #1's nice suggestion, we have added the suggested quantitative investigation in Line 243-268 as follows:

In order to quantitatively describe the effects of neutral temperature and meridional neutral winds, we calculate the 630-nm airglow intensity by integrating the volume emission rate along the altitude. So we make two new plots [Fig. (a) and Fig. (b)] to show how the integrated emission rates vary with the increasing neutral temperature and neutral winds, respectively. Fig. (a) shows the result regarding the integrated emission rate as affected by neutral temperature (at -5° geomagnetic latitude on February 1, 2007). The curve in red is fitted as 2<sup>nd</sup>-order polynomial :

$$S = (0.1354 \pm 0.0069)(\Delta T) - (4.6835 \pm 0.2652) \times 10^{-4}(\Delta T)^2 ,$$

where  $S$  ( $\text{km}/(\text{cm}^3 * \text{s})$ ) is the change in integrated emission rate and  $\Delta T$  (K) is

the increase in neutral temperature, compared with the standard conditions of 650 K neutral temperature and zero neutral wind.

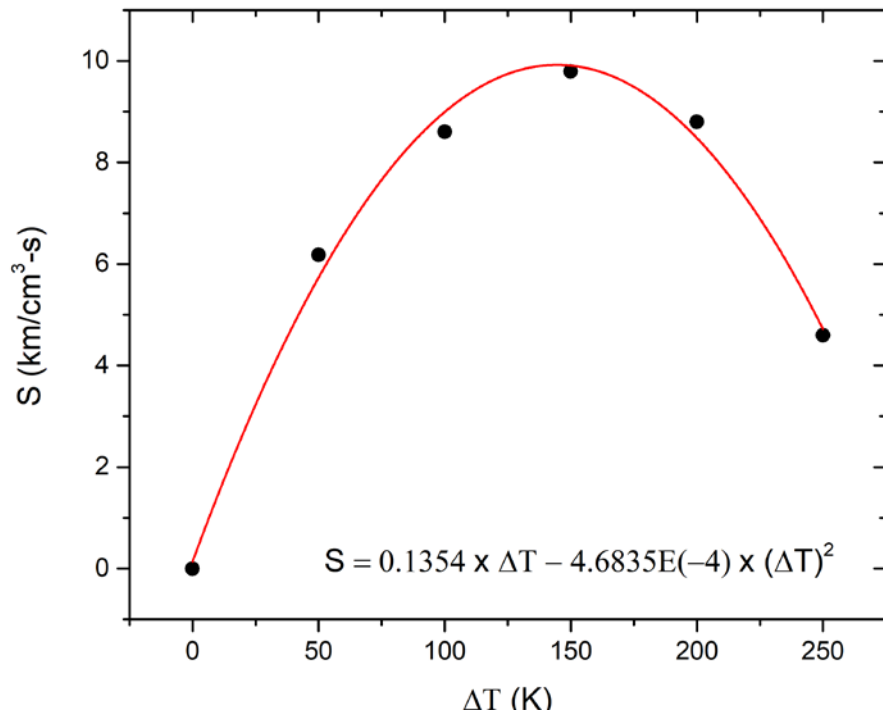


Figure (a)

Fig. (b) shows the result regarding the integrated emission rate as affected by neutral wind. The results are obtained based on the same standard conditions as those considered in Fig. (a). The curve in red fits an exponential function :

$$S = (64.8883 \pm 0.7772) \times \{1 - \exp[-(0.0885 \pm 0.0041)(\Delta W)]\} ,$$

where  $S$  (km/(cm<sup>3</sup> \* s)) is the change in integrated emission rate and  $\Delta W$  (m/s) is the change in neutral wind velocity.

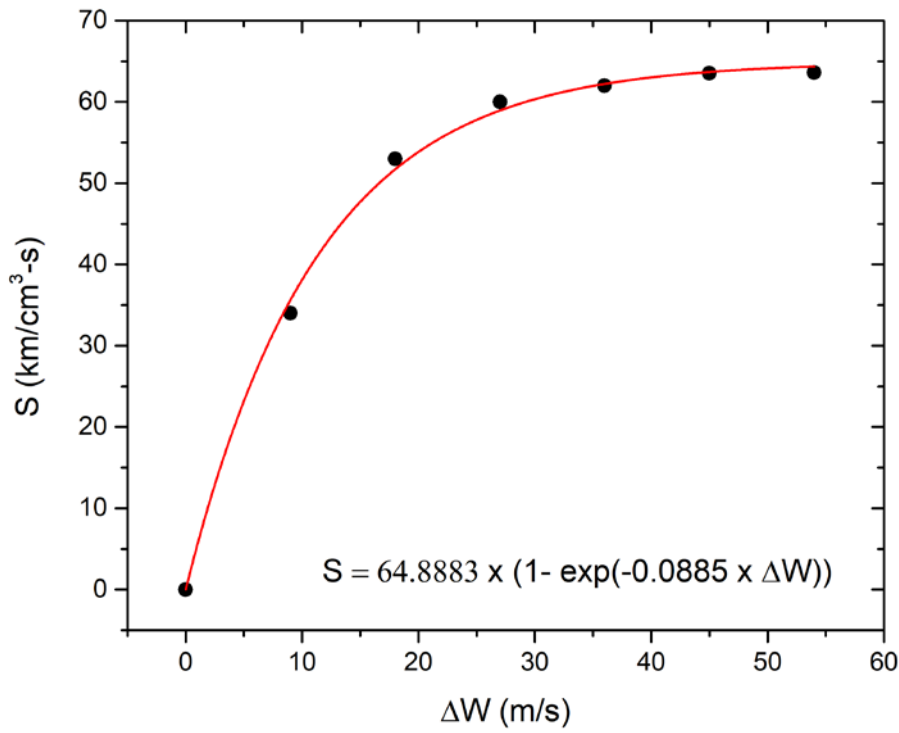


Figure (b)

Therefore, we combine the results of the two fitting functions to approximate the overall change in the integrated emission rate due to the two effects:

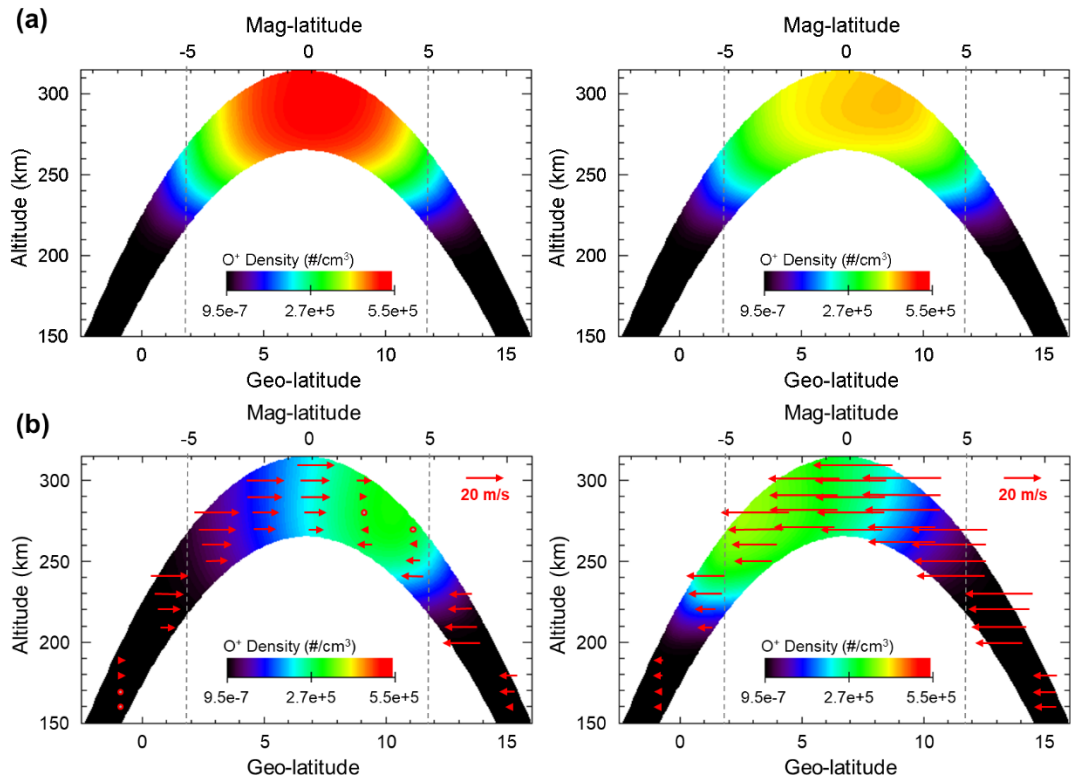
$$S = 0.1354(\Delta T) - 4.6835 \times 10^{-4}(\Delta T)^2 + 64.8883[1 - \exp(-0.0885(\Delta W))]$$

Based on the function, we can quantitatively compare the neutral temperature effect with the neutral wind effect. In Fig. (a), the maximum change of the integrated emission rate by increasing the neutral temperature is 9.7859 (km/(cm<sup>3</sup> \* s)) at 145 K. To get the same changes of the emission rate by varying the neutral wind, it just requires a neutral wind velocity of 1.85 m/s. Above such a velocity, the neutral wind effect would certainly be larger than that of the neutral temperature for this case.

Minor comments:

- Figure 1: Arrows representing wind velocity is not seen clearly.

We have replotted the Fig. 1 as follows, thank you.



- L. 916, Figure 2  $\rightarrow$  Figure 3

Our manuscript does not have Line 916. We searched all the “Figure 2” in our article but did not find a similar typo as mentioned. If Referee #1 can still identify the typo, please let us know again. We would revise it. Thank you.

## Anonymous Referee #2

Chiang et al. demonstrate the influence of meridional wind and neutral temperature to the intensity of 630.0 nm nightglow around the equatorial midnight, altering the SAMI2 model for the resulting plasma density and temperature with the inputs from NRLMSISE-00 for neutral densities and the HWM-93 for neutral wind vectors. The work is potentially interesting and novelty to the community, particularly the finding with respect to the neutral temperature. However, the literature survey by the authors seems to be hasty, the major lacking is that the role of meridional wind to the midnight 630.0 nm airglow enhancement seeing by ISUAL Imager has been studied and published (Rajesh et al.(2014) doi 10.1002/2014JA019927). In addition, the manuscript requires an editing for English before it can be published in the peer-review journal. Given the interesting result and a very valuable dataset, I encourage the authors in extending the content in greater detail that be able to deliver the science finding clearly. Please see further comment below. Summary: Consider for publication after substantial revision Major points:

We thank the Reviewer for reading our article carefully and providing many valuable suggestions for improving the manuscript. We revise the manuscript by taking into account the Reviewer's comments. We also extend the contents and include the observation results in this manuscript in accordance with the Reviewer's suggestions.

(1) Observation data Since the satellite data are used, it would be appropriate to cite Frey et al.(2016) (doi 10.1002/2016JA022616) for the instrument details and the first results of the limb imaging of 630.0 nm airglow using ISUAL by Rajesh et al. (doi 10.1029/2009JA014087 ). The authors put the observation data in the Supplement for some reasons, but it could be nicer if move the section to the main content. The observation data deserve more attention and discussion.

The main purpose of this study is to understand the influence of temperature and meridional neutral wind on the 630.0 nm nightglow by calculating the volume emission rates. The observations by ISUAL can help us realize the tendency in typical solstice condition. In our previous manuscript, we merely wanted to state that our simulations can easily reproduce the selected short-period cases of the brightness patterns observed by ISUAL. But case-study results are not our main points. Considering the observational data that we can access, we suggest that statistical analyses are a more appropriate method to unveil the midnight brightness mechanism.

So in the previous manuscript, we put the observation data in the Supplement. Since Referee #2 thinks that the observation data deserve more attention and discussion, we agree to move them to the main contents in Line 275-286. Moreover, we also add the two references suggested by Referee #2 in Line 53-56 and references section.

(2) The effect of meridional winds to the 630.0 nm midnight brightness By reading this work and Rajesh et al. (2014), I happened to find many similarities in between. Both of the groups modulate the HWM-93 meridional winds on the SAMI2 model and apparently find that the meridional wind utilizes the location and intensity of the airglow brightness. What is the novelty of this work out of Rajesh et al. (2014) in the effect of meridional winds to the midnight brightness? The authors should include the comparison in the content and give the credit to the previous work properly.

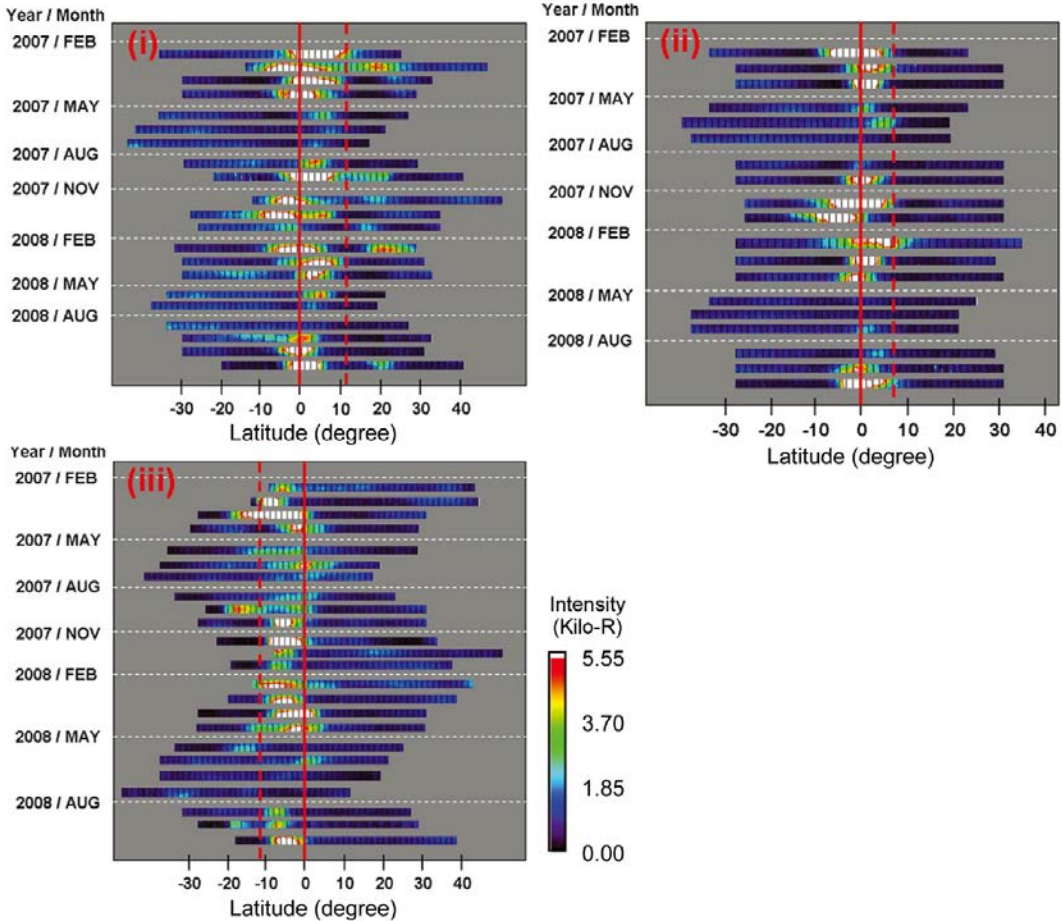
We thank the Referee's suggestion. We discuss the differences in detail between the work by Rajesh et al. [2014] and our study. In our manuscript, we include the following discussion in Line 299-315 to compare the two studies.

Rajesh et al. [2014] showed their simulation results and claimed that using merely the background meridional winds could reproduce the observed brightness. They selected a few cases of ISUAL image data and compared those data with the simulation results by the SAMI2 model. Nevertheless, using such a method by Rajesh et al. [2014], one should be very careful about the details when it comes to physical insights or conclusions drawn from the study. This is because ISUAL only provided optical data and there was not any instrument on the satellite to directly observe the relevant conditions (temperature, wind field, etc.) in the environment. Without such observations to provide constraints for modeling, one can easily reproduce similar-looking results of selected short-period data by adjusting modeling parameters in simulations. However, images seemingly similar to that of an ISUAL observation could be produced from simulation results using considerably different parameter values, which may correspond to different dominant mechanisms. Thus, when there are few constraints for the parameter values, roughly comparing a short-period case of ISUAL image data with simulation results without paying attention to details may lead to an interpretation of brightness production mechanisms that is different from the real situation.

The production mechanisms of 630-nm bright spot around midnight from ISUAL observations have been explained by Adachi et al. [2010]. Adachi et al. [2010] suggested the midnight temperature maximum (MTM) effect can well explain the bright spot based on the observation timing and brightness locations. Our previous

research (Chiang et al. [2013]) also reached similar conclusions based on statistical studies using two years of ISUAL data. The brightness region tends to appear between the geographic equator and magnetic equator as Fig. 5 in Chiang et al. [2013] indicates (see figure below). This figure shows the sequencing data observed from different longitudinal regions by ISUAL. The dotted red lines indicate the geomagnetic equator; the solid red lines indicate the geographic equator. Rajesh et al. [2014] claimed that the production mechanism of midnight brightness can be explained by meridional winds. The brightness region in their simulation results, however, basically appeared on the winter side of the magnetic equator in the solstices due to the summer-to-winter wind, regardless of where the geographic equator was. Thus, with the consideration of the location of the geographic equator, which is a significant physical factor associated with the MTM effect, the observation results of Fig. 5 in Chiang et al. [2013] indicated that the real situation would actually be different from the case simulated by Rajesh et al. [2014]. Thus the production mechanisms of midnight brightness require different interpretations from those provided by Rajesh et al. [2014].

Thus, we propose that the production of midnight brightness should not be explained by considering merely the effect of meridional neutral wind. Both temperature change and meridional neutral wind can lead to variations of the 630.0 nm nightglow intensity while the latter is more effective. These two effects should be taken into account in the study of midnight brightness.



Note: Fig. 5 in Chiang et al. [2013] shows the observations from three different longitudinal regions [(i), (ii) and (iii)] that correspond to the different declination angles. Orbit (i) was in the longitudinal region (between  $-15^\circ \sim +150^\circ$  longitude) where the geomagnetic equator is northward of the geographic equator with the declination angle around  $0^\circ$ . Orbit (iii) was in the region (between  $-85^\circ \sim -60^\circ$  longitude) with the geomagnetic equator southward of the geographic equator and the declination angle around  $0^\circ$ . Orbit (ii) was in the geographic region between  $-60^\circ \sim -15^\circ$  longitude, with a declination angle around  $-20^\circ$  (westward). The solid lines and dashed lines indicate the geographic equator and geomagnetic equator, respectively.

Line 116-117 What is special of O+ density along the magnetic line with apex altitude between 265 and 315 km ? Can you show the model result between altitude 150 to 315 km for all latitude?

Sorry for our typo. We have modified this sentence to “Figure 1 shows the O+ density along the magnetic lines with altitudes between 150 and 315 km in the latitude-altitude plane at the time and longitude described above” in Line 118-120.

Line 214-226 Again, what is the new finding out of fig.3 in Rajesh et al. (2014) ?

Figure 3 in Rajesh et al. [2014] shows statistical results of midnight brightness for different seasons using all the ISUAL images. They collected all the airglow mode data to consider the occurrence of the brightness region but they did not separate the situations for different longitudinal regions.

As we explained in our response to the previous question, Fig. 5 in Chiang et al. [2013] indicates that the latitudinal locations of brightness observed from 3 different orbits (different longitudes) are quite different. We need to consider both temperature change and meridional neutral wind such that the production of midnight brightness in different longitudinal regions can be appropriately addressed. Thus, the statistical results of Fig. 3 in Rajesh et al. [2014] can be considered preliminary work to address the production of midnight brightness, but a broader study to include more relevant physics, such as one also considering the physical factors related to the longitudes, is warranted so as to improve our understanding on the topic. This is also the reason why our study in this manuscript just focuses on the specific longitudinal regions.

Figure 1 has to be modified, what is the reason that the authors didn't convert [O+] density to volume emission rate of 630.0 nm nightglow while the observation images are the airglow intensities?

The effects of neutral wind and temperature on the volume emission rate of the 630.0 nm nightglow are shown in Fig. 2 in our manuscript. The volume emission rate of the 630.0 nm nightglow in the F2 region can be derived as follows:

$$I_{630} = \frac{A_{1D}\mu_D\gamma[O_2][O^+]}{k_1[N_2] + k_2[O_2] + k_3[O] + A_{1D} + A_{2D}}$$

It shows that the volume emission rate is associated with neutral and charged densities. Charged density can be shifted along the field line by neutral wind. On the other hand, most of the items, including charged density, neutral densities and chemical reaction rates, can be affected by temperature variation. Here we would like to explain the thread of thoughts in describing Fig. 1 and Fig. 2. In the context, we first let readers understand the neutral wind effect on charged densities (as shown in Fig. 1), and subsequently we show the effects of neutral wind and temperature on the volume emission rate of the 630.0 nm nightglow (as shown in Fig. 2). Referee #2 suggested that we plot volume emission rate instead of [O+] density in Figure 1. If we plot volume emission rate as suggested, that means both the neutral wind effect and temperature effect need to be considered in Figure 1. Thus it will require lots of figures to show the results because temperature changes need to be considered. We

are afraid that readers would be confused by the large number of plots in such an early part of the manuscript, and thus it might not be easy for them to understand our points. Therefore, we tend to keep Fig. 1 as it is shown in the previous manuscript.

Minor points line by line:

Line 43 enhancement > increase

Thank you. We have revised it in Line 43.

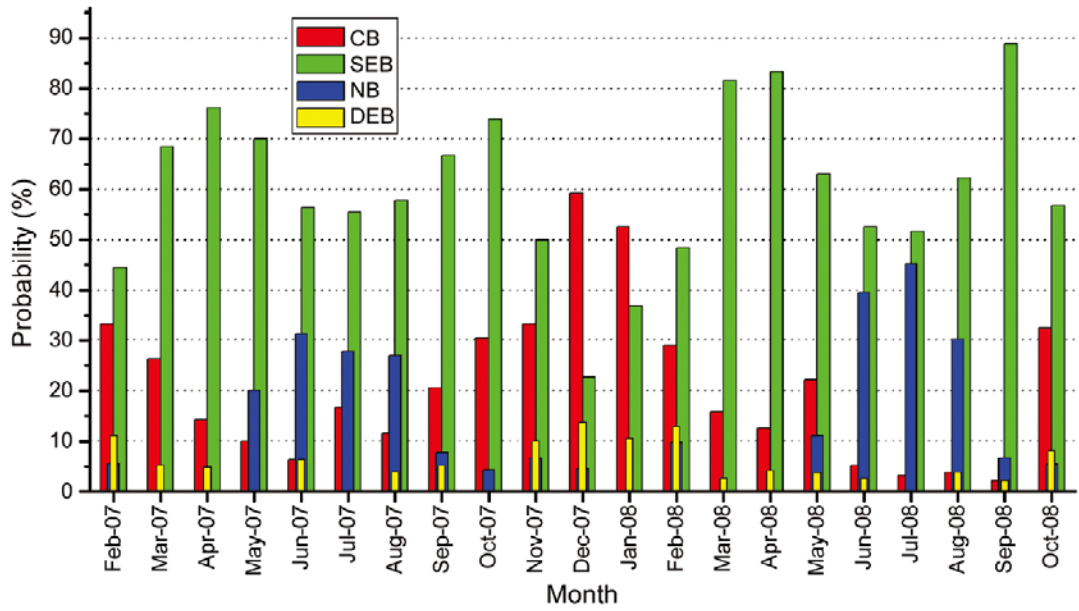
Line 45-46 "first reported the MTM" should be "reported the MTM phenomenon first"

Thank you. We have revised it in Line 45.

Line 61 What are the different mechanisms addressed in Chiang et al. (2013)? The readers would be pleased to learn the relevant work leading by the same author.

Thanks for the Reviewer's comment, we have put the sentence in Line 60-67.

The following figure is Fig. 6 in Chiang et al. [2013]. In the paper, our major goals are to investigate the different patterns of midnight brightness observed by ISUAL and to consider the possible mechanisms for all kinds of cases. Occurrence rates of the four brightness types from all the orbits in each month are shown in the figure: single equatorial brightness (SEB) cases are in green, double equatorial brightness (DEB) in yellow, conjugate brightness (CB) in red, and no brightness (NB) in blue. We found that midnight brightness was controlled by different sources at different locations. First, NB was associated with the ionospheric annual anomaly during May to July. Second, we suppose that SEB and DEB were associated primarily with the MTM effect and the featured temperature variation. Third, the CB case, however, was associated largely with the winter anomaly which the neutral wind plays a role in its formation. It is necessary to take into account the locations and seasons when explaining the mechanisms of midnight brightness occurrence. Overall, the global midnight brightness can be contributed by several effects including the influence of the MTM effect, summer-to-winter neutral wind and ionospheric anomaly.



Line 142-143 Rewrite the sentence please.

Thanks for the Reviewer's comment, we have rewritten the sentence in Line 144-147 as follows:

"In order to explore the effects of temperature change, we modify the codes of SAMI2 by increasing 50 K per run as the inputs, and perform the simulations to calculate the emission intensity values associated with different temperature conditions."

Line 193-195 Rewrite the sentence please.

Thanks for the Reviewer's comment, we have rewritten the sentence in Line 185-187 as follows:

"Therefore, we suggest that the low-latitude emission enhancement in the winter hemisphere be achieved by plasma accumulation brought about by the summer-to-winter neutral wind."

Line 202-203 Rewrite the sentence please.

Thanks for the Reviewer's comment, we have rewritten the sentence in Line 204-207 as follows:

"In comparison, the change due to temperature variation is just 0.015 photon/cm<sup>3</sup>/sec for every K. The ratio of the two numbers is 46. Consideration of

other conditions, such as those cases shown in Fig. 2, may reduce the corresponding ratio, but it should still be at least 20.”

1 Variations of the 630.0 nm airglow emission with meridional  
2 neutral wind and neutral temperature around midnight

3 Chih-Yu Chiang<sup>1</sup>, Sunny Wing-Yee Tam<sup>1</sup>, Tzu-Fang Chang<sup>1,2</sup>

4 <sup>1</sup> Institute of Space and Plasma Sciences, National Cheng Kung University, Tainan  
5 70101, Taiwan

6 <sup>2</sup> Institute for Space-Earth Environmental Research, Nagoya University, Nagoya  
7 464-8601, Japan

8     **Abstract**

9         The ISUAL payload onboard the FORMOSAT-2 satellite has often observed  
10         airglow bright spots around midnight at equatorial latitudes. Such features had been  
11         suggested as the signature of thermospheric midnight temperature maximum (MTM)  
12         effect, which was associated with temperature and meridional neutral winds. This  
13         study investigates the influence of neutral temperature and meridional neutral wind on  
14         the volume emission rates of the 630.0 nm nightglow. We utilize the SAMI2 model to  
15         simulate the charged and neutral species at the 630.0 nm nightglow emission layer  
16         under different temperatures with and without the effect of neutral wind. The results  
17         show that the neutral wind is more efficient than temperature variation in affecting the  
18         nightglow emission rates. However, the emission rate features a local maximum in its  
19         variation with the temperature. Two kinds of tendencies can be seen regarding the  
20         temperature that corresponds to the turning point, which is named the turning  
21         temperature ( $T_t$ ) in this study: firstly,  $T_t$  decreases with the emission rate for the same  
22         altitude; secondly, for approximately the same emission rate,  $T_t$  increases with the  
23         altitude.

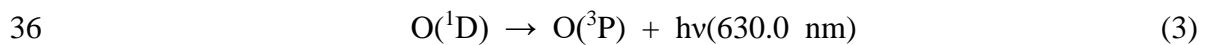
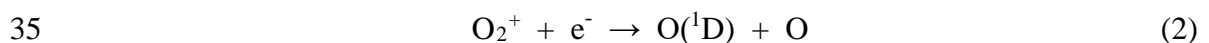
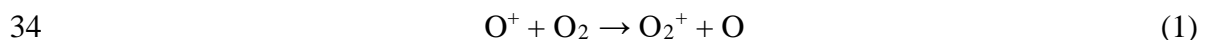
24

25

26

27 1. Introduction

28 The atomic oxygen red line at 630.0 nm is the most prominent emission in the  
29 nighttime ionosphere. It usually forms an emission layer in the F region at altitudes of  
30 ~200–300 km and can be easily observed from ground-based observatories or  
31 satellites [Nelson and Cogger, 1971; Kelley *et al.*, 2002; Thuillier *et al.*, 2002]. The  
32 emission is related to O(<sup>1</sup>D), whose production in the nighttime is mainly via the  
33 charge exchange and dissociative chemical processes listed as follows:



37 Based on the  $[O^+] \sim N_e$  (electron density) approximation [Peterson *et al.*, 1966;  
38 *Link and Cogger, 1988*] in the F2 region, the intensity of the OI(<sup>1</sup>D) 630.0 nm spectral  
39 line is usually used to identify the ionospheric electron density variations. From a rich  
40 history in the literature, the intensity of OI(<sup>1</sup>D) 630.0 nm airglow emissions is known  
41 as Midnight Brightness Wave (MBW) [*Herrero and Meriwether, 1980; Herrero et al.,*  
42 *1993; Colerico et al., 1996; Colerico and Mendillo, 2002*].

43 During occurrences of MBW, **increase** in temperature are usually observed  
44 around local midnight, which are termed Midnight Temperature Maximum (MTM)  
45 effect. *Harper* [1973] and *Spencer et al.* [1979] **reported the MTM phenomenon first.**

46 The cases in their studies were observed by the incoherent scatter radar from Arecibo  
47 and the NATE experiment aboard the Atmospheric Explorer E (AE-E) satellite,  
48 respectively. The amplitude of the temperature bulge was found to range from 20 to  
49 200 K [Spencer *et al.*, 1979; Burnside *et al.*, 1981; Colerico and Mendillo, 2002;  
50 Meriwether *et al.*, 2008]. In addition, a number of studies about midnight brightness  
51 have reported the relation between *in-situ* temperature and neutral wind measurements  
52 [e.g., Herrero and Meriwether, 1980; Sastri *et al.*, 1994, Colerico *et al.*, 1996, 2002;  
53 Otsuka *et al.*, 2003; Mukherjee *et al.*, 2006]. Rajesh *et al.* [2009] showed the first  
54 results of the limb image of 630.0 nm airglow using Imager of Sprites and Upper  
55 Atmospheric Lightning (ISUAL) [Chang *et al.*, 2012; Chiang *et al.*, 2013; Frey *et al.*,  
56 2016] on board the FORMOSAT-2 satellite. Adachi *et al.* [2010] also showed a  
57 14-day time span of airglow observations obtained from the Asian sector by ISUAL.  
58 On the basis of the observation time and location, they suggested that the equatorial  
59 airglow probably corresponded to the midnight brightening wave (MBW) which is in  
60 association with the occurrence of MTM. Furthermore, Chiang *et al.* [2013]  
61 statistically investigated the global midnight brightness according to seasons and  
62 found that the global midnight brightness near the equatorial regions was controlled  
63 by different mechanisms. In the study, the features and behavior of the 630.0 nm  
64 midnight intensity were investigated by analyzing the optical images obtained by

65 ISUAL. Cases of global midnight brightness were successfully categorized into four  
66 types that were mainly due to the influence of temperature changes, neutral wind and  
67 ionospheric anomaly.

68 Based on the previous studies, it is known that temperature and meridional  
69 neutral wind are correlated and associated with manifestations of MTM. Thus, we  
70 want to discuss these two effects at the same time. In this study, we calculate the volume  
71 emission rates to understand the influence of neutral temperature and meridional  
72 neutral wind on the 630.0 nm nightglow. We shall discuss the sensitivities of the  
73 emission rates to the temperature and the densities of several neutral and charged  
74 species. Moreover, some new features will also be shown in the discussion section.  
75 And we also provide ISUAL observation results to show that our calculation results  
76 are reasonable and realistic.

77

## 78 **2. Model features**

79 Temperature changes and meridional neutral wind can influence the O(<sup>1</sup>D)  
80 nightglow intensity through particle densities. The volume emission rate of the 630.0  
81 nm nightglow in the F2 region [Sobral *et al.*, 1993] can be derived from the chemical  
82 process of 630.0 nm nightglow (Supplement I). It is shown as follows:

$$83 I_{630} = \frac{A_{1D}\mu_D\gamma[O_2][O^+]}{k_1[N_2] + k_2[O_2] + k_3[O] + A_{1D} + A_{2D}} , \quad (4)$$

84 where  $\mu_D$  is the quantum yield of O(<sup>1</sup>D), which is about 1~1.3 [Torr and Torr, 1982];  
85  $\gamma$  is the rate coefficient of Reaction (1) [St.-Maurice and Torr, 1978];  $k_1$ ,  $k_2$  and  $k_3$  are  
86 the rate coefficients of O(<sup>1</sup>D) quenched by N<sub>2</sub>, O<sub>2</sub> and O, respectively [Langford *et al.*,  
87 1986; Streit *et al.*, 1976; Sun and Dalgarno, 1992]; and  $A_{1D}$  and  $A_{2D}$  are the transition  
88 coefficients [Froese-Fischer and Saha, 1983]. The formulas for the rate coefficients  
89 [Vlasov *et al.*, 2005] are listed in Table 1. The production rate of O(<sup>1</sup>D) is contributed  
90 by the oxygen ion density [O<sup>+</sup>] and the molecular oxygen density [O<sub>2</sub>] through the  
91 linked reactions (1) and (2). The major loss rates of O(<sup>1</sup>D) are associated with the  
92 densities of molecular oxygen [O<sub>2</sub>], molecular nitrogen [N<sub>2</sub>], and atomic oxygen [O],  
93 as reflected in Eq. (4). The densities [O<sup>+</sup>], [O<sub>2</sub>], [N<sub>2</sub>] and [O] and the rate coefficients  
94  $\gamma$ ,  $k_1$ ,  $k_2$  and  $k_3$  all depend on temperature. In addition, [O<sup>+</sup>] may change with the  
95 neutral wind conditions. In order to determine  $I_{630}$  under different temperatures and  
96 neutral wind conditions, one must first determine the densities of the relevant species.  
97 In this study, [O<sup>+</sup>] and plasma temperatures under various conditions are found by the  
98 SAMI2 model of the Naval Research Lab [Huba *et al.*, 2000]. SAMI2 is a two-  
99 dimensional, first-principle model of the comprehensive low to mid-latitude  
100 ionosphere. SAMI2 code includes most of the mechanisms that should be considered  
101 in the ionosphere. There are photoionizations, chemical process, effects by the  
102 magnetic and electric fields, plasma dynamics and the influence from the neutral

103 atmosphere. The input variables, neutral species, are specified using the empirical  
104 codes, the Mass Spectrometer Incoherent Scatter model (NRLMSISE-00) [Picone *et*  
105 *al.*, 2002] for neutral densities and the Horizontal Wind Model (HWM-93) [Hedin *et*  
106 *al.*, 1996] for neutral wind. The continuity and momentum equations of seven ion  
107 species ( $H^+$ ,  $He^+$ ,  $N^+$ ,  $O^+$ ,  $N_2^+$ ,  $NO^+$ , and  $O_2^+$ ) are solved in the code.

108 In order to understand the differences due to the meridional neutral wind, we  
109 apply the SAMI2 model with and without neutral wind by changing the multiplicative  
110 factor of neutral wind (tvn0) to see the differences between two solstices. Thus, we  
111 simulate the cases of February 1, 2007 (northern winter) and August 1, 2007 (northern  
112 summer). In the simulations, we suppose that the solar and geomagnetic activities are  
113 in quiet conditions (F10.7 index = 60, Ap index = 7). The simulations are run for the  
114 altitude range between 150 and 1000 km from  $-30^\circ$  to  $+30^\circ$  geomagnetic latitudes.  
115 Inside this region, we use 100 geomagnetic field lines and 201 grid points along **each**  
116 field line. Our report of the results will focus on the locations at  $-5^\circ$  and  $+5^\circ$   
117 geomagnetic latitude ( $+2^\circ$  and  $+12^\circ$  geographic latitude respectively) along the 100°E  
118 geographic longitude, which intersects these latitudes in the Asian region. **Figure 1**  
119 **shows the  $O^+$  density along the magnetic lines with altitudes between 150 and 315 km**  
120 **in the latitude-altitude plane at the time and longitude described above.** Figure 1(a)  
121 shows the results under the condition that lacks neutral wind, and Fig. 1(b) shows the

122 results with the effect of normal neutral wind. The two left panels are for February 1,  
123 2007 and the two right panels are for August 1, 2007. The arrows plotted in Fig. 1(b)  
124 indicate the strength and directions of the meridional neutral wind. Comparison of Fig.  
125 1(a) and 1(b) clearly shows that meridional winds transport the plasma along the  
126 magnetic field line and change the plasma density distribution. And this change of the  
127 plasma profile could directly modify the emission rate in Eq. (4). The dashed lines,  
128 which correspond to  $\pm 5^\circ$  geomagnetic latitude, indicate the locations where the  
129 intensity of the 630.0 nm nightglow is examined in detail in this study.

130

### 131 **3. Results and Analysis**

132 Based on Eq. (4),  $I_{630}$  under different temperatures and different neutral wind  
133 conditions is plotted in Fig. 2. The neutral wind conditions for the results in Fig. 2 are  
134 the same as those for Fig. 1. The strength and directions of the neutral winds are  
135 indicated by the arrows shown in Fig. 1. The simulation results shown in the figure  
136 are for (a) February 1, 2007 and (b) August 1, 2007, with the left and right panels  
137 respectively corresponding to  $-5^\circ$  and  $+5^\circ$  geomagnetic latitude. The letters, A, B, C,  
138 D and E, indicate the altitudes of 220, 230, 240, 250 and 260 km, respectively. The  
139 dotted lines indicate the results with normal neutral wind effect; the solid lines  
140 indicate the results without neutral wind effect. Note that the temperatures of around

141 650 K, corresponding to the leftmost points of the lines in the figure, were the initial  
142 neutral temperatures obtained from the NRLMSISE-00 model at the various altitudes.  
143 These neutral temperatures are input into the SAMI2 model, and we set up the  
144 48-hour data as a running loop to obtain the plasma data. In order to explore the  
145 effects of temperature change, we modify the codes of SAMI2 by increasing 50 K per  
146 run as the inputs, and perform the simulations to calculate the emission intensity  
147 values associated with different temperature conditions.

148 From Fig. 2, we can see the influence of temperature and neutral wind on the  
149 nightglow emission. Note that the neutral wind conditions are as in Fig. 1: Fig. 1(a)  
150 for zero wind condition and Fig. 1(b) for normal wind condition. The influence of the  
151 temperature variations on  $I_{630}$  is usually less than 3 photons/cm<sup>3</sup>/sec at the heights of  
152 220 to 260 km. The variation of  $I_{630}$  with temperature, however, is not monotonic;  
153 there is a maximum in the intensity as the temperature changes. In terms of height, as  
154  $I_{630}$  depends on the local neutral and charged particle densities in accordance with Eq.  
155 (4), the emission is the strongest at 230 km, except for the condition of very weak  
156 emission (< 1 photon/cm<sup>3</sup>/sec) that occurs at +5° geomagnetic latitude in August with  
157 normal wind effect (right panel of Fig. 2(b)).

158 As for the influence of the neutral wind on February 1, 2007 (Fig. 2(a)), both  
159 locations ( $\pm 5^\circ$  geomagnetic latitude) clearly feature significantly smaller  $I_{630}$  under

160 this effect. We suggest that this is due to the meridional neutral wind blowing  
161 equatorward in both hemispheres (see Fig. 1) and pushing the plasma upward along  
162 the field lines, reducing the local charged particle densities and consequently the  
163 emission rates as well. On August 1, 2007, as shown in Fig. 2(b), the neutral wind  
164 causes the intensity at  $+5^\circ$  geomagnetic latitude to decrease significantly for the same  
165 reason as the wind direction is locally southward (equatorward). This southward  
166 neutral wind, however, has an opposite effect on the intensity at  $-5^\circ$  geomagnetic  
167 latitude; being locally poleward, the wind pushes the plasma downward along the  
168 field lines, increasing the local charged particle densities and consequently the  
169 emission rates as well.

170 From Eq. (4), we can see that  $I_{630}$  is related to the densities of several neutral  
171 species as well. In order to find out how the temperature affects the overall chemical  
172 process that leads to the 630.0 nm emission, a few relevant parameters are shown as  
173 functions of temperature in Fig. 3, based on the condition at 230 km altitude and  $-5^\circ$   
174 geomagnetic latitude on February 1, 2007. In Fig. 3(a), the  $\text{O}({^1}\text{D})$  loss-rate terms  
175 associated with  $[\text{O}]$ ,  $[\text{N}_2]$  and  $[\text{O}_2]$ , are shown in dotted, dashed and solid lines  
176 respectively. The term  $\gamma [\text{O}^+][\text{O}_2]$ , which is related to the  $\text{O}({^1}\text{D})$  production rate and  
177 is in the numerator of Eq. (4), is plotted in Fig. 3(b). The dotted line represents the  
178 normal neutral wind condition, and the solid line for the windless condition.

179

180 **4. Discussion**

181 From Fig. 1(a), we can see that along the field lines, the O<sup>+</sup> density is maximum  
182 around the geomagnetic equator when there is no neutral wind, whether it is in the  
183 summer or winter season. But the [O<sup>+</sup>] maxima tilt to the winter hemisphere in the  
184 presence of summer-to-winter neutral wind at the geomagnetic equator, as shown in  
185 Fig. 1(b). **Therefore, we suggest that the low-latitude emission enhancement in the**  
186 **winter hemisphere be achieved by plasma accumulation brought about by the**  
187 **summer-to-winter neutral wind.**

188 From the results that include the normal wind effect as shown in Fig. 2, the  
189 intensities on opposite sides of the geomagnetic equator are very different. The  
190 weaker emission is in the summer hemisphere, and brightness of higher intensity  
191 appears in the winter hemisphere. In previous studies, *Rishbeth and Setty* [1961]  
192 found that NmF2 was larger in winter than in summer, and they first suggested the  
193 possibility of composition change being the cause of the winter anomaly. *Rishbeth*  
194 [1972] and *Torr and Torr* [1973] suggested that the anomaly might be due to  
195 transequatorial neutral wind blowing from the summer hemisphere to the winter  
196 hemisphere. Therefore, the enhancement of the emission at the low latitudes of the  
197 winter hemisphere should be the results of plasma accumulation caused by the neutral

198 wind effect.

199 Figure 2 shows the influence of temperature and neutral wind on the nightglow  
200 emission rates. We estimate the intensity change under different neutral wind  
201 conditions based on the location at 230 km altitude and  $-5^{\circ}$  geomagnetic latitude on  
202 February 1, 2007. In this situation, the emission would be reduced by the wind flow,  
203 and the average change is about 0.690 photon/cm<sup>3</sup>/sec for every m/sec of the wind  
204 speed. In comparison, the change due to temperature variation is just 0.015  
205 photon/cm<sup>3</sup>/sec for every K. The ratio of the two numbers is 46. Consideration of  
206 other conditions, such as those cases shown in Fig. 2, may reduce the corresponding  
207 ratio, but it should still be at least 20. According to earlier studies, the neutral wind  
208 speed is generally 0-300 m/sec in the F region [Dyson *et al.*, 1997], while the  
209 amplitude of the temperature bulge due to the MTM effect has been found to range  
210 from 20 to 200 K [Burnside *et al.*, 1981; Colerico and Mendillo, 2002]. Even if one  
211 assumes the maximum wind speed is just 60 m/sec as in the simulations in this study,  
212 it would require a temperature change of 1200 K to match the same change in  
213 emission intensity caused by the neutral wind. Such a large temperature change is not  
214 realistic in comparison with the maximum observed difference of 200 K. Thus, the  
215 emission rate of nightglow, realistically, is influenced more by the neutral wind than  
216 temperature change when the former mechanism is clearly present.

217 The densities and some of the rate coefficients are temperature dependent, as  
218 given in Eq. (4). We analyze the change with temperature of the individual terms in  
219 Eq. (4). In Fig. 3(a) and Fig. 3(b), we **plot** the terms in the numerator and denominator  
220 on the right-hand side of Eq. (4) and **find** that all these terms increase with  
221 temperature. However, if we consider the derivative of the terms with respect to  
222 temperature, which characterizes how sensitive the terms are to temperature change,  
223 we notice that the derivatives for  $k_1[N_2]$  and  $k_3[O]$  increase with temperature while  
224 those for  $k_2[O_2]$  and  $\gamma [O^+][O_2]$  decrease, as shown in Fig. 3(a) and 3(b). How the  
225 variations of these terms affect the dependence of  $I_{630}$  on temperature can now be  
226 understood from the right-hand side of Eq. (4). In particular, the numerator, which  
227 characterizes the production rate of  $O(^1D)$  and is proportional to  $\gamma [O^+][O_2]$ ,  
228 increases with temperature while featuring a relatively large increase at lower  
229 temperatures (less than  $\sim 750$  K). On the other hand, the denominator, which  
230 characterizes the total loss rate of  $O(^1D)$  and is dominated by  $k_1[N_2]$  as Fig. 3(a)  
231 indicates, features a relatively large increase at higher temperatures (larger than  $\sim 750$   
232 K). Upon division of the numerator by the denominator, the plot of  $I_{630}$  vs.  
233 temperature is thus characterized by quasi-parabolic lines with the presence of a local  
234 maximum --- or a turning point in the curve --- as shown in Fig. 2. We refer to the  
235 temperature that corresponds to such a local maximum as the turning temperature ( $T_t$ ).

236 Below  $T_t$ ,  $I_{630}$  increases with temperature, meaning that the increase in the production  
237 of  $O(^1D)$  associated with a rise in the temperature is more efficient than the increase in  
238 its loss. In contrast,  $I_{630}$  decreases with temperature above  $T_t$ , meaning that the  
239 increase in the production of  $O(^1D)$  associated with a rise in the temperature is less  
240 efficient than the increase in its loss. Thus,  $T_t$  has the significance of being the  
241 temperature at which the production and loss rates of  $O(^1D)$  are equally sensitive to a  
242 temperature change.

243 In order to quantitatively describe the effects of neutral temperature and  
244 meridional neutral winds, we calculate the 630-nm airglow intensity by integrating the  
245 volume emission rate along the altitude. Figure 4(a) and 4(b) show how the integrated  
246 emission rates vary with the increasing neutral temperature and neutral winds,  
247 respectively. Fig. 4(a) shows the result regarding the integrated emission rate as  
248 affected by neutral temperature (at  $-5^\circ$  geomagnetic latitude on February 1, 2007). The  
249 curve in red is fitted as 2<sup>nd</sup>-order polynomial :

$$250 \quad S = (0.1354 \pm 0.0069)(\Delta T) - (4.6835 \pm 0.2652) \times 10^{-4}(\Delta T)^2,$$

251 where  $S$  ( $km/(cm^3 * s)$ ) is the change in integrated emission rate and  $\Delta T$  (K) is  
252 the increase in neutral temperature, compared with the standard conditions of 650 K  
253 neutral temperature and zero neutral wind. Fig. 4(b) shows the result regarding the  
254 integrated emission rate as affected by neutral wind. The results are obtained based on

255 the same standard conditions as those considered in Fig. 4(a). The curve in red fits an  
256 exponential function :

257 
$$S = (64.8883 \pm 0.7772) \times \{1 - \exp[-(0.0885 \pm 0.0041)(\Delta W)]\},$$

258 where  $S$  (km/(cm<sup>3</sup> \* s)) is the change in integrated emission rate and  $\Delta W$  (m/s)  
259 is the change in neutral wind velocity. Therefore, we combine the results of the two  
260 fitting functions to approximate the overall change in the integrated emission rate due  
261 to the two effects:

262 
$$S = 0.1354(\Delta T) - 4.6835 \times 10^{-4}(\Delta T)^2 + 64.8883[1 - \exp(-0.0885(\Delta W))],$$

263 Based on the function, we can quantitatively compare the neutral temperature effect  
264 with the neutral wind effect. In Fig. 4(a), the maximum change of the integrated  
265 emission rate by increasing the neutral temperature is 9.7859 (km/(cm<sup>3</sup> \* s)) at 145  
266 K. To get the same changes of the emission rate by varying the neutral wind, it just  
267 requires a neutral wind velocity of 1.85 m/s. Above such a velocity, the neutral wind  
268 effect would certainly be larger than that of the neutral temperature for this case.

269 Figure 5 shows a plot of  $T_t$  versus the emission rate  $I_{630}$  at specific altitudes. The  
270 results include all the cases shown in Fig. 2 with different symbols indicating different  
271 altitudes. Two kinds of tendencies can be seen from the plot: firstly,  $T_t$  decreases with  
272  $I_{630}$  for the same altitude; secondly, for approximately the same emission rate,  $T_t$   
273 increases with the altitude. This is the first result to show these tendencies of the

274 turning temperature.

275 Observations have found cases that are consistent with our simulation results  
276 regarding the influence of the neutral wind. Figure 6 shows four cases observed by  
277 ISUAL in the Asian region at 23:00 local time during the two months considered in  
278 our studies: two cases in February shown on the left side and two cases in August  
279 shown on the right side. Figure 6(a) would be for the condition of no wind or weak  
280 wind while Fig. 6(b) would correspond to the normal wind condition. We can see  
281 from Fig. 6(a) that a bright spot of nightglow was observed at the geomagnetic  
282 equator during both months. As the volume emission rate, according to Eq. (4), is  
283 proportional to the  $O^+$  density, the observations were supportive of the simulation  
284 results of density variations in Fig. 1(a). Similarly, the two cases in Fig. 6(b), which  
285 featured nightglow bright spots in the winter hemisphere, suggested that the density  
286 variations shown in Fig. 1(b) are realistic.

287 Previously, Chiang et al. [2013] examined the occurrence rates of global  
288 midnight brightness observed by ISUAL. In order to verify the enhancement of the  
289 emission intensity in the winter hemisphere by the neutral wind, we examined the  
290 ISUAL data that correspond to the specific regions and seasons considered in our  
291 simulations and the results are shown in Fig. 7(a) and (b). We found that among the  
292 22 valid observation days during January and February, ~77% of the days featured the

293 appearance of nightglow bright spots in the low-latitude region of the winter  
294 hemisphere (Fig. 7(a)). Furthermore, ~83% of the 30 valid observation days during  
295 July-August also featured nightglow bright spots at low latitudes in the corresponding  
296 winter hemisphere (Fig. 7(b)). Thus, statistical results regarding the location of  
297 nightglow bright spots agree with the simulation results that demonstrate the crucial  
298 role of the neutral wind in affecting the location of high-intensity nightglow regions.

299 *Rajesh et al. [2014]* showed their simulation results and claimed that using  
300 merely the background meridional winds could reproduce the observed brightness.  
301 They selected a few cases of ISUAL image data and compared those data with the  
302 simulation results by the SAMI2 model. Nevertheless, using such a method by Rajesh  
303 et al. [2014], one should be very careful about the details when it comes to physical  
304 insights or conclusions drawn from the study. This is because ISUAL only provided  
305 optical data and there was not any instrument on the satellite to directly observe the  
306 relevant conditions (temperature, wind field, etc.) in the environment. Without such  
307 observations to provide constraints for modeling, one can easily reproduce  
308 similar-looking results of selected short-period data by adjusting modeling parameters  
309 in simulations. However, images seemingly similar to that of an ISUAL observation  
310 could be produced from simulation results using considerably different parameter  
311 values, which may correspond to different dominant mechanisms. Thus, when there

312 are few constraints for the parameter values, roughly comparing a short-period case of  
313 ISUAL image data with simulation results without paying attention to details may  
314 lead to an interpretation of brightness production mechanisms that is different from  
315 the real situation.

316 Observations of the movement of MTM temperature bulge and that of nightglow  
317 have led to postulations of an association between pressure bulge and nightglow  
318 intensity [*Colerico et al.*, 1996; *Colerico and Mendillo*, 2002; *Meriwether et al.*,  
319 2008]. However, the high intensities of the observed nightglow have not been  
320 successfully reproduced using existing models incorporating the MTM effect, such as  
321 the NCAR thermosphere-ionosphere-electrodynami general circulation model  
322 (TIEGCM), as pointed out by *Colerico and Mendillo* [2002] and *Meriwether et al.*  
323 [2008]. Note that temperature was not included as a varying quantity in traditional  
324 ionospheric models. Thus the simulation study of temperature effect upon nightglow  
325 intensity is lacking. Our simulation results have demonstrated the unexpectedly  
326 non-monotonic dependence of the intensity of nightglow on the neutral temperature,  
327 with the turning temperature  $T_t$  that arises from the dependence implying a limitation  
328 for the growth of the emission rates. As the temperature increases above  $T_t$ , the  
329 emission rates do not continue to grow. In fact, temperature change such as in the case  
330 of heat transfer is affected by the density, which controls the heat capacity. At the

331 same time, temperature change may generate pressure difference and lead to transport  
332 that changes density profiles. As nightglow intensity depends also on particle densities,  
333 its non-monotonic variations with temperature are in fact due to the combination of  
334 temperature and density. While our study suggests that neutral wind is the dominant  
335 **driver** of the  $I_{630}$  variation, its influence, however, is via transportation of plasma and  
336 neutral particles, in which case consideration of the effect of temperature on the  
337 density is essential. Moreover, it has not been established that MTM is affected by the  
338 wind primarily. The combination of temperature and density, which has shown to  
339 cause non-monotonic results in this study, may very well be an important factor in the  
340 study of MTM. Thus, if one wants to fully reproduce the observation results, we  
341 suggest other extra factors associated with temperature variations should also be  
342 considered, such as different tidal modes from lower atmosphere [Akmaev *et al.*,  
343 2009]. Our findings of the turning temperature tendencies can help as a guide for  
344 choosing the background temperature in future modeling attempts to obtain intensities  
345 of nightglow brightness comparable to those observed from ground or from space.  
346 *Shepherd* [2016] investigates the possible extent of the MTM at  $\sim 20^{\circ}\text{N}$ – $40^{\circ}\text{N}$ ,  
347 considering O(1D) airglow volume emission rates, Doppler temperatures, and neutral  
348 **wind** (zonal and meridional) observations by the Wind Imaging Interferometer  
349 (WINDII) experiment on board the Upper Atmosphere Research Satellite (UARS).

350 Their results provide us the relations of the zonal wind to the O(1D) emission rate and  
351 of the meridional wind to the temperature. Such relations potentially guide us to  
352 design a more extensive future study in simulation so as to reproduce the observation  
353 and statistical results by *Shepherd [2016]*.

354

## 355 **5. Conclusion**

356 Previous studies of the MTM effect have pointed out that the temperature  
357 anomaly influences the nighttime behavior of the thermosphere. And the neutral wind  
358 also plays a key role to cause the intensity variations in the nighttime ionosphere.  
359 Based on our simulation results, both temperature change and meridional neutral wind  
360 could cause the 630.0 nm nightglow intensity to vary while the latter is more effective.

361 And the simulation results may successfully explain most of the observational results  
362 by ISUAL. An unexpected aspect of the results is the non-monotonic dependence of  
363 the emission rate on temperature, featuring a turning point as the temperature changes.  
364 The temperature  $T_t$  at which the turning point occurs corresponds to a balanced  
365 condition between the production and loss of O(1D). Thus, our results help understand  
366 how the overall chemical process of nightglow is affected by the variations of neutral  
367 temperature and neutral wind. Two kinds of tendencies can be seen regarding the  
368 turning temperature  $T_t$ . One is the higher  $T_t$  corresponding to higher altitude at the

369 same emission rate, the other is the higher  $T_t$  corresponding to lower emission rate at  
370 the same altitude. Our findings of these turning temperature tendencies can guide  
371 future modeling attempts to match the observed nightglow brightness intensities.

372

373 **Acknowledgements**

374 The authors acknowledge the FORMOSAT-2/ISUAL science and operator team  
375 to provide image data (<http://sprite.phys.ncku.edu.tw/en/about-cdf-distribution>). The  
376 work by C. Y. Chiang and S. W. Y. Tam is supported by Taiwan's Ministry of Science  
377 and Technology grants MOST105-2111-M-006-007. T. F. Chang acknowledges  
378 support by the Ministry of Education, Taiwan R.O.C., from The Aim for the Top  
379 University Project to National Cheng Kung University.

380

381

382

383

384

385

386

387

388 **References**

389 Adachi, T., M. Yamaoka, M. Yamamoto, Y. Otsuka, H. Liu, C.-C. Hsiao, A. B. Chen,  
390 and R.-R. Hsu (2010), Midnight latitude-altitude distribution of 630-nm airglow  
391 in the Asian sector measured with FORMOSAT-2/ISUAL, *J. Geophys. Res.*,  
392 doi:10.1029/2009JA015147.

393 Akmaev, R. A., F. Wu, T. J. Fuller-Rowell, and H. Wang (2009), Midnight  
394 temperature maximum (MTM) in Whole Atmosphere Model (WAM)  
395 simulations, *Geophys. Res. Lett.*, 36, L07108, doi:10.1029/2009GL037759.

396 Burnside, R. G., F. A. Herrero, J. W. Meriwether Jr., and J. C. G. Walker (1981),  
397 Optical observations of thermospheric dynamics at Arecibo, *J. Geophys. Res.*,  
398 86, 5532.

399 Chang, T. F., C. Z. Cheng, C. Y. Chiang, and A. B. Chen (2012), Behavior of substorm  
400 auroral arcs and Pi2 waves: Implication for the kinetic ballooning instability,  
401 *Ann. Geophys.*, 30, 911–926, doi:10.5194/angeo-30-911-2012.

402 Chiang, C. Y., T. F. Chang, S. W.-Y. Tam, T. Y. Huang, A. B.-C. Chen, H. T. Su, and R.  
403 R. Hsu (2013), Global observations of the 630-nm nightglow and patterns of  
404 brightness measured by ISUAL. *Terr. Atmos. Ocean. Sci.*, 24, 283-293, doi:  
405 10.3319/TAO.2012.12.13.01(SEC)

406 Colerico, M., M. Mendillo, D. Nottingham, J. Baumgardner, J. Meriwether, J. Mirick,

407 B. W. Reinisch, J. L. Scali, C. G. Fesen, and M. A. Biondi (1996), Coordinated  
408 measurements of F region dynamic related to the thermospheric midnight  
409 temperature maximum, *J. Geophys. Res.*, 101, 26,783–26,793.

410 Colerico, M. J., and M. Mendillo (2002), The current state of investigations regarding  
411 the thermospheric midnight temperature maximum (MTM), *J. Atmos. Sol. Terr.  
412 Phys.*, 64, 1361– 1369.

413 Dyson, P. L., T. P. Davies, M. L. Parkinson, A. J. Reeves, P. G. Richards, and C. E.  
414 Fairchild (1997), Thermospheric neutral winds at southern mid-latitudes: A  
415 comparison of optical and ionosonde hmF2 methods, *J. Geophys. Res.*,  
416 102(A12), 27189–27196, doi:10.1029/97JA02138.

417 Frey, H. U., et al. (2016), The Imager for Sprites and Upper Atmospheric Lightning  
418 (ISUAL), *J. Geophys. Res. Space Physics*, 121, 8134–8145,  
419 doi:10.1002/2016JA022616.

420 Froese-Fischer, C., and H. P. Saha (1983), Multiconfiguration Hartree-Fock results  
421 with Breit-Pauli corrections for forbidden transitions in the 2p4 configuration,  
422 *Phys. Rev. A*, 28, 3169– 3178.

423 Harper, R. M. (1973), Nighttime meridional neutral winds near 350 km at low to  
424 mid-latitudes, *J. Atmos. Terr. Phys.*, 35, 2023– 2034.

425 Hedin, A.E., E.L. Fleming, A.H. Manson, F.J. Schmidlin, S.K. Avery, R.R. Clark, S.J.

426 Franke, G.J. Fraser, T. Tsuda, F. Vial, and R.A. Vincent (1996), Empirical wind  
427 model for the upper, middle, and lower atmosphere, *J. Atmos. Terr. Phys.*, 58,  
428 1421-1447.

429 Herrero, F. A., and J. W. Meriwether Jr. (1980), 6300 airglow meridional intensity  
430 gradients, *J. Geophys. Res.*, 85, 4191.

431 Herrero, F. A., N. W. Spencer, and H. G. Mayr (1993), Thermosphere and F-region  
432 plasma dynamics in the equatorial region, *Adv. Space Res.*, 13(1), 201–220.

433 Huba, J. D., G. Joyce, and J. A. Fedder (2000), Sami2 is another model of the  
434 ionosphere (SAMI2): A new low-latitude ionosphere model, *J. Geophys. Res.*,  
435 105, 23,035–23,053.

436 Kelley, M. C., J. J. Makela, B. M. Ledvina, and P. M. Kintner (2002), Observations of  
437 equatorial spread F from Haleakala, Hawaii, *Geophys. Res. Lett.*, 29(20), 2003,  
438 doi:10.1029/2002GL015509.

439 Langford, A. O., V. M. Bierbaum, and S. R. Leone (1986), Branching ratios for  
440 electronically excited oxygen atoms formed in the reaction of N+ with O2 at  
441 300 K, *J. Chem. Phys.*, 84, 2158– 2166.

442 Link, R., and L. L. Cogger (1988), A reexamination of the OI 6300 Å nightglow, *J.*  
443 *Geophys. Res.*, 93(A9), 9883-9892.

444 Meriwether, J., Faivre, M., Fesen, C., Sherwood, P., and Veliz, O (2008), New results

445 on equatorial thermospheric winds and the midnight temperature maximum,  
446 *Ann. Geophys.*, 26, 447–466.

447 Mukherjee, G. K., N. Parihar, K. Niranjan, and G. Manju (2006), Signature of  
448 midnight temperature maximum (MTM) using OI 630 nm airglow, *Indian J.*  
449 *Radio Space Phys.*, 35, 14–21.

450 Nelson, G. J., and L. L. Cogger (1971), Dynamical behavior of the nighttime  
451 ionosphere at Arecibo, *J. Atmos. Terr. Phys.*, 33, 1711 – 1726,  
452 doi:10.1016/0021-9169(71)90219-4.

453 Otsuka, Y., T. Kadota, K. Shiokawa, T. Ogawa, S. Kawamura, S. Fukao, and S.-R.  
454 Zhang (2003), Optical and radio measurements of a 630-nm airglow  
455 enhancement over Japan on 9 September 1999, *J. Geophys. Res.*, 108(A6), 1252,  
456 doi:10.1029/2002JA009594.

457 Peterson, V. L., T. E. Van Zandt, and R. B. Norton (1966), F-region nightglow  
458 emissions of atomic oxygen, 1. Theory, *J. Geophys. Res.*, 71, 2255–2265.

459 Picone, J. M., A. E. Hedin, D. P. Drob, and A. C. Aikin (2002), NRLMSISE-00  
460 empirical model of the atmosphere: Statistical comparisons and scientific issues,  
461 *J. Geophys. Res.*, 107(A12), 1468, doi:10.1029/2002JA009430

462 Rajesh, P. K., J. Y. Liu, C. Y. Chiang, A. B. Chen, W. S. Chen, H. T. Su, R. R. Hsu, C.  
463 H. Lin, M.-L. Hsu, J. H. Yee, and J. B. Nee (2009), First results of the limb

464 imaging of 630.0 nm airglow using FORMOSAT-2/Imager of Sprites and Upper  
465 Atmospheric Lightnings, J. Geophys. Res., 114, A10302,  
466 doi:10.1029/2009JA014087.

467 Rajesh, P. K., C. H. Chen, C. H. Lin, J. Y. Liu, J. D. Huba, A. B. Chen, R. R. Hsu, and  
468 Y. T. Chen (2014), Low-latitude midnight brightness in 630.0 nm limb  
469 observations by FORMOSAT-2/ISUAL, J. Geophys. Res. Space Physics,  
470 4894–4904, 119, doi:10.1002/2014JA019927.

471 Rishbeth, H., and C. S. G. K. Setty (1961), The F layer at sunrise, *J. Atmos. Terr.  
472 Phys.*, 20, 263-267.

473 Rishbeth, H. (1972), Thermospheric winds and the F-region – A review, *J. Atmos. Terr.  
474 Phys.*, 34, 1.

475 Sastri, J. H., H. N. R. Rao, V. V. Somayajulu, and H. Chandra, Thermospheric winds  
476 associated with equatorial midnight temperature maximum (MTM), *Geophys.  
477 Res. Lett.*, 21, 825, 1994.

478 Shepherd, M. G. (2016), WINDII observations of thermospheric O(1D) nightglow  
479 emission rates, temperature, and wind: 1. The northern hemisphere midnight  
480 temperature maximum and the wave 4, *J. Geophys. Res. Space Physics*, 121,  
481 doi:10.1002/2016JA022703.

482 Sobral, J. H.A., H. Takahashi, M. A. Abdu, P. Muralikrishna, Y. Sahai, C. J. Zamlutti,

483 E. R. de Paula, and P. P. Batista (1993), Determination of the quenching rate of  
484 the O(<sup>1</sup>D) by O(<sup>3</sup>D) from rocket-borne optical (630 nm) and electron density  
485 data, *J. Geophys. Res.*, 98, 7791-7798.

486 Spencer, N. W., C. R. Carignan, H. G. Mayr, H. B. Niemann, R. F. Theis, and L. E.  
487 Wharton (1979), The midnight temperature maximum in the Earth's equatorial  
488 thermosphere, *Geophys. Res. Lett.*, 6, 444.

489 St. Maurice, J. P., D. G. Tort, Nonthermal rate coefficients in the ionosphere: The  
490 reactions of O<sub>2</sub><sup>+</sup> with N<sub>2</sub>, O<sub>2</sub>, and NO, *J. Geophys. Res.*, 83, 969, 1978.

491 Streit, G. E., C. J. Howard, A. L. Schmeltekopf, J. J. A. Davidson, and H. I. Schiff  
492 (1976), Temperature dependence of O(1D) rate constants for reactions with O<sub>2</sub>,  
493 N<sub>2</sub>, CO<sub>2</sub>, O<sub>3</sub> and H<sub>2</sub>O, *J. Chem. Phys.*, 65, 4761– 4764.

494 Sun, Y., and A. Dalgarno (1992), Collisional excitation of metastable O(1D) atoms, *J.*  
495 *Chem. Phys.*, 96, 5017– 5019.

496 Thuillier, G., R. H. Wiens, G. G. Shepherd, and R. G. Roble (2002), Photochemistry  
497 and dynamics in thermospheric intertropical arcs measured by the WIND  
498 Imaging Interferometer on board UARS: A comparison with TIE-GCM  
499 simulations, *J. Atmos. Sol. Terr. Phys.*, 64, 405– 415,  
500 doi:10.1016/S1364-6826(01)00109-2.

501 Torr, M. R. and D. G. Torr (1973), The seasonal behaviour of the F2-layer of the

502 ionosphere, *J. Atmos. Terr. Phys.*, 35, 2237.

503 Torr, M. R. and D. G. Torr (1982), The role of metastable species in the

504 thermosphere, *Rev. Geophys. and Space Phys.*, **20**, 91–144.

505 Vlasov, M. N., M. J. Nicolls, M. C. Kelley, S. M. Smith, N. Aponte, and S. A.

506 Gonzalez (2005), Modeling of airglow and ionospheric parameters at Arecibo

507 during quiet and disturbed periods in October, 2002, *J. Geophys. Res.*, 110,

508 A07303, doi:10.1029/2005JA011074.

509

510

511

512

513

514

515

516

517

518

519

520

521 Table 1. Reactions and rate coefficients related to the volume emission rate of the  
 522 630.0 nm airglow

Reactions	Rate Coefficients (cm <sup>3</sup> s <sup>-1</sup> , s <sup>-1</sup> )
O <sup>+</sup> + O <sub>2</sub> → O <sub>2</sub> <sup>+</sup> + O	$\gamma = 2.82 \times 10^{-11} - 7.74 \times 10^{-12} (T_{\text{eff}}/300) + 1.07 \times 10^{-12} (T_{\text{eff}}/300)^2 - 5.17 \times 10^{-14} (T_{\text{eff}}/300)^3 + 9.65 \times 10^{-16} (T_{\text{eff}}/300)^4$
O( <sup>1</sup> D) + N <sub>2</sub> → O + N <sub>2</sub>	$k_1 = 2 \times 10^{-11} \exp(107.8/T_n)$
O( <sup>1</sup> D) + O <sub>2</sub> → O + O <sub>2</sub>	$k_2 = 2.9 \times 10^{-11} \exp(67.5/T_n)$
O( <sup>1</sup> D) + O → O + O	$k_3 = (3.73 + 1.1965 \times 10^{-1} T_n^{0.5} - 6.5898 \times 10^{-4} T_n) \times 10^{-12}$
O( <sup>1</sup> D) → O + hν(630.0nm)	$A_{1D} = 7.1 \times 10^{-3}$
O( <sup>1</sup> D) → O + hν(634.4nm)	$A_{2D} = 2.2 \times 10^{-3}$

523 Note:  $T_{\text{eff}} = 0.67T_i + 0.33T_n$  ( $T_{\text{eff}}$  : effective temperature,  $T_i$ : ion temperature,  $T_n$ : neutral  
 524 temperature) [St.-Maurice and Torr, 1978]

525

526

527

528

529

530

531

532

533

534

535

536

537

538 **Figure Captions**

539 Figure 1. Oxygen ion density plotted in the latitude-altitude plane at 23:00 LT on  
540 February 1, 2007 (left panels) and August 1, 2007 (right panels) in the Asian  
541 region (100°E longitude) from the SAMI-2 model: (a) without neutral wind; (b)  
542 with the effect of normal neutral wind, whose strength and directions are  
543 indicated by the arrows.

544 Figure 2. The results of 630.0 nm emission rate at 23 LT at different temperatures and  
545 under different neutral wind conditions for (a) February 1, 2007 and (b) August  
546 1, 2007: left and right panels respectively for -5° and +5° geomagnetic latitude;  
547 the letters, A, B, C, D and E, for the altitudes of 220 km, 230 km, 240 km, 250  
548 km and 260 km, respectively; for normal neutral wind effect (black dotted lines)  
549 and windless conditions (red solid lines). The neutral wind conditions of Fig. 2  
550 are the same as those shown in Fig. 1.

551 Figure 3. Profiles of the terms in Eq. (4) that are associated with neutral and charged  
552 species versus temperature, based on 230 km altitude and -5° geomagnetic  
553 latitude on February 1, 2007, with and without neutral wind: (a) the loss-rate  
554 terms associated with [O], [N<sub>2</sub>] and [O<sub>2</sub>]; (b) the production-rate term  $\gamma$   
555 [O<sup>+</sup>][O<sub>2</sub>].

556 **Figure 4.** Quantitative results for how (a) the neutral temperature and (b) the neutral

557 wind affect the 630-nm airglow intensity.

558 Figure 5. Plots of the emission rates against the turning temperature between 220-260

559 km altitudes.

560 Figure 6. Four observation cases by ISUAL in February 2007 and August 2007 (the

561 same periods as shown in Fig. 1).

562 Figure 7. ISUAL data in the specific regions and seasons considered in the

563 simulations: the nightglow bright spots in valid observation days during (a)

564 January-February and (b) July-August.

565

566

567

568

569

570

571

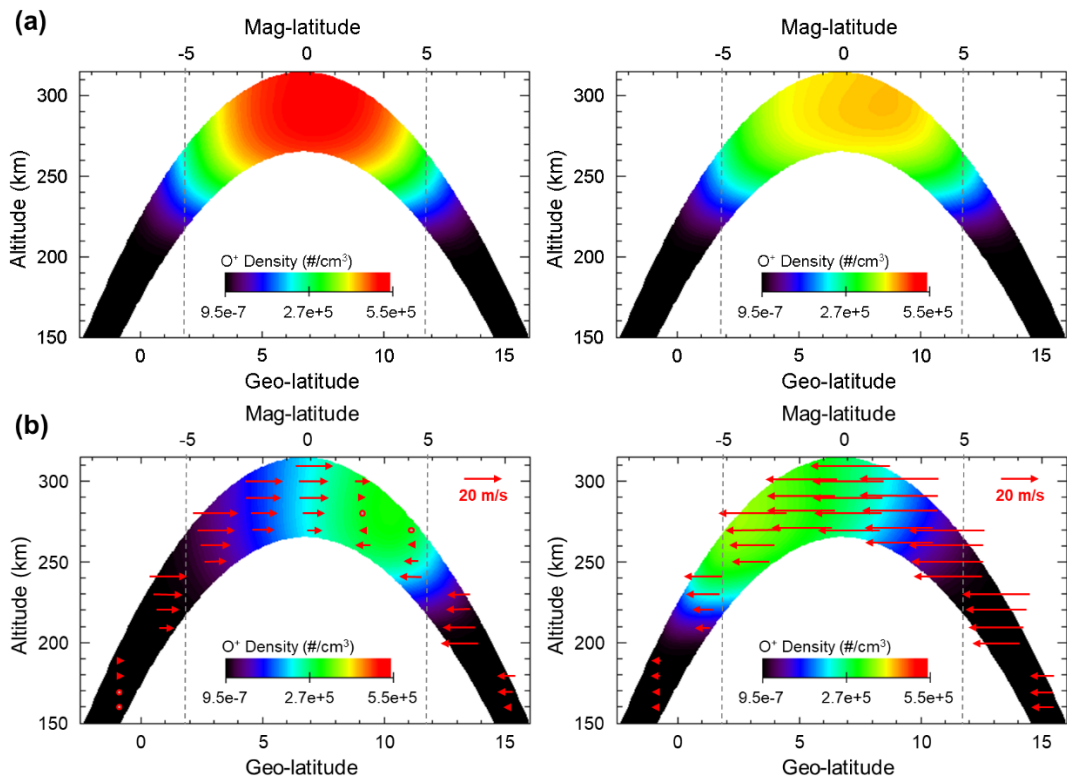
572

573

574

575

576 **Figure 1**



577

578

579

580

581

582

583

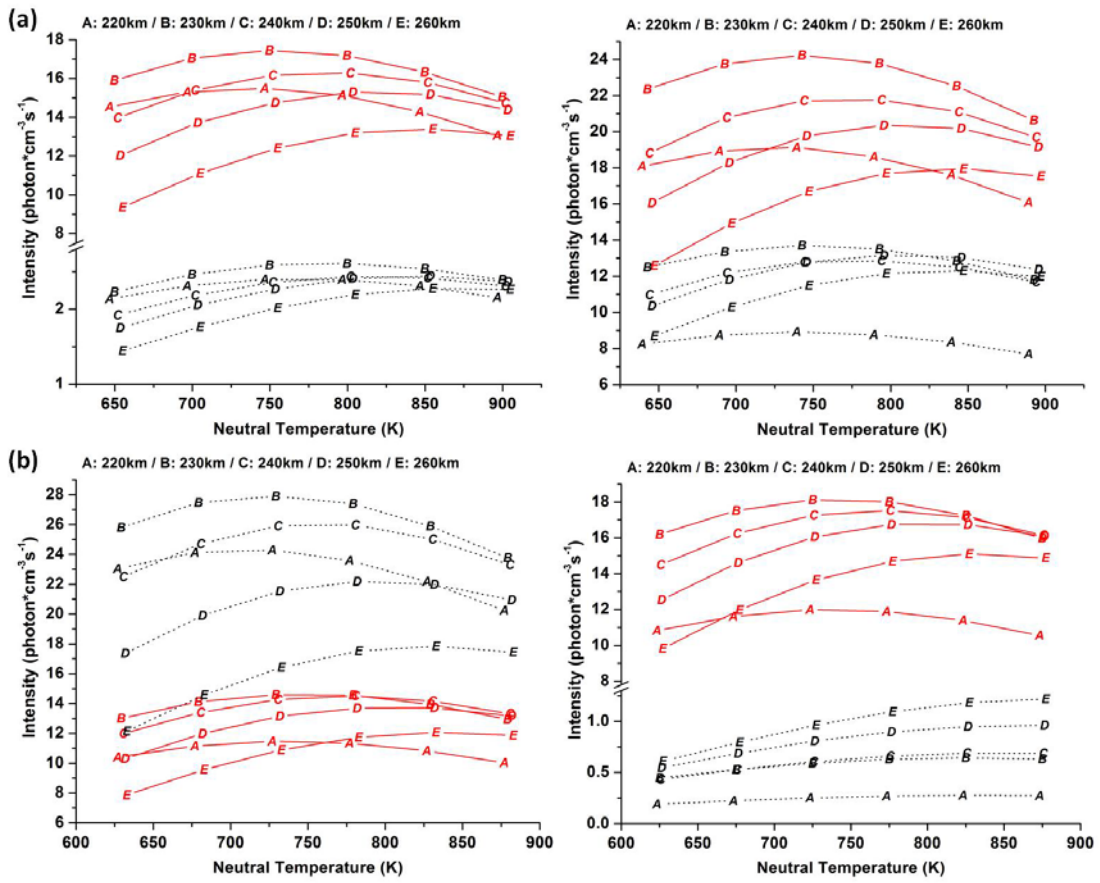
584

585

586

587

588 Figure 2



589

590

591

592

593

594

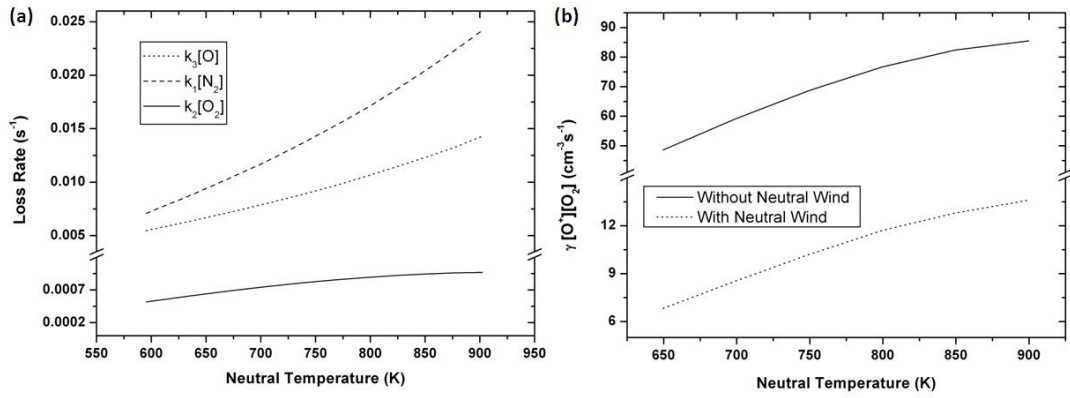
595

596

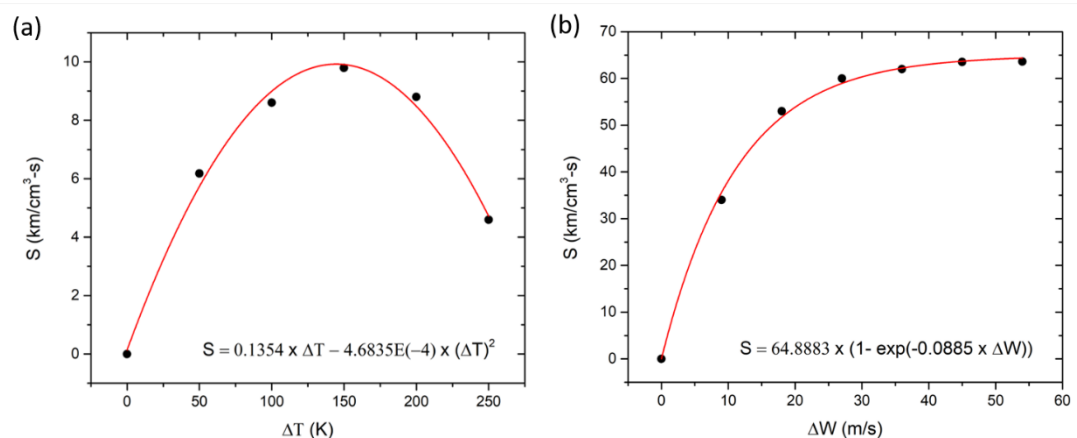
597

598

599      Figure 3



615 **Figure 4**



616

617

618

619

620

621

622

623

624

625

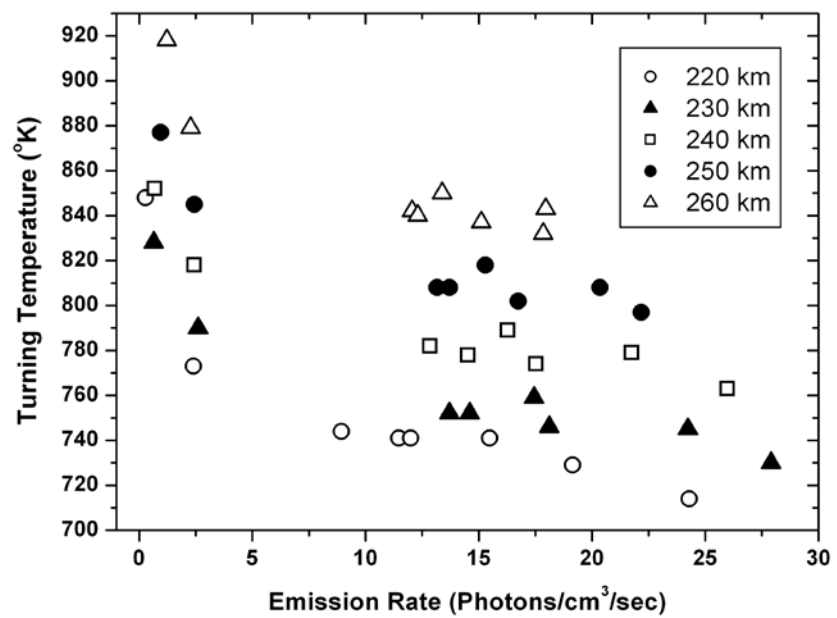
626

627

628

629

630 Figure 5



631

632

633

634

635

636

637

638

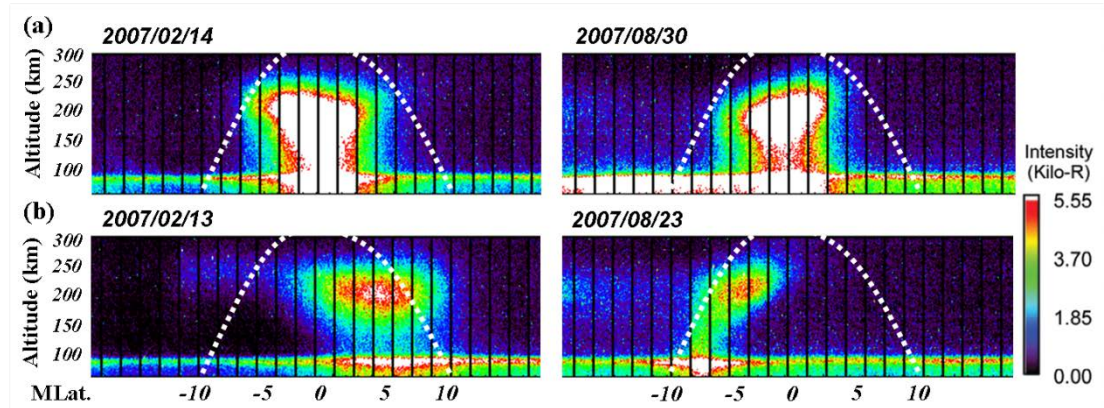
639

640

641

642

643 **Figure 6**



644

645

646

647

648

649

650

651

652

653

654

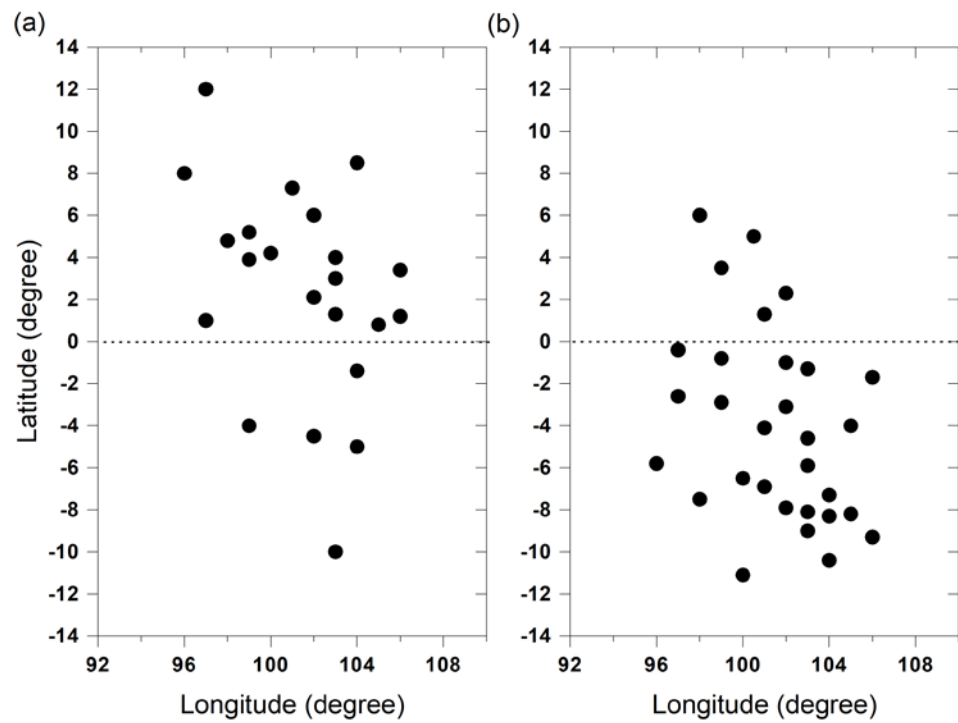
655

656

657

658

659 **Figure 7**



660

661